Malaria Journal

RESEARCH

Open Access

Monitoring individual rice field flooding dynamics over a large scale to improve mosquito surveillance and control

Mauricianot Randriamihaja[1,2,3*†], Tokiniaina M. Randrianjatovo[1,2†], Michelle V. Evans[1,2,4], Felana A. Ihantamalala[1,4], Vincent Herbreteau[5], Christophe Révillion[6,7], Eric Delaitre[6], Thibault Catry[6] and Andres Garchitorena[1,2]

Abstract

Background Progress in malaria elimination has been hindered by recent changes in mosquito behaviour and increased insecticide resistance in response to traditional vector control measures, such as indoor residual spraying and long-lasting insecticidal nets. There is, therefore, increasing interest in the use of larval source management (LSM) to supplement current insecticide-based interventions. However, LSM implementation requires the characterization of larval habitats at fine spatial and temporal scales to ensure interventions are well-placed and well-timed. Remotely sensed optical imagery captured via drones or satellites offers one way to monitor larval habitats remotely, but its use at large spatio-temporal scales has important limitations.

Methods A method using radar imagery is proposed to monitor flooding dynamics in individual rice fields, a primary larval habitat, over very large geographic areas relevant to national malaria control programmes aiming to implement LSM at scale. This is demonstrated for a 3971 km^2 malaria-endemic district in Madagascar with over 17,000 rice fields. Rice field mapping on *OpenStreetMap* was combined with Sentinel-1 satellite imagery (radar, 10 m) from 2016 to 2022 to train a classification model of radar backscatter to identify rice fields with vegetated and open water, resulting in a time-series of weekly flooding dynamics for thousands of rice fields.

Results From these time-series, over a dozen indicators useful for LSM implementation, such as the timing and frequency of flooding seasons, were obtained for each rice field. These monitoring tools were integrated into an interactive GIS dashboard for operational use by vector control programmes, with results available at multiple scales (district, sub-district, rice field) relevant for different phases of LSM intervention (e.g. prioritization of sites, implementation, follow-up).

Conclusions Scale-up of these methods could enable wider implementation of evidence-based LSM interventions and reduce malaria burdens in contexts where irrigated agriculture is a major transmission driver.

Keywords Health surveillance system, *OpenStreetMap* mapping, Synthetic aperture radar, Larval source management, Decision-making tools, Malaria

†Mauricianot Randriamihaja and Tokiniaina M. Randrianjatovo have contributed eqaully.

*Correspondence:
Mauricianot Randriamihaja
mauricianothr@gmail.com
Full list of author information is available at the end of the article

Background

Sustained progress in the global fight against malaria has been achieved in recent decades. A keystone of this effort has been the scale-up of insecticide-based vector control measures, such as indoor residual spraying and long-lasting insecticidal nets in malaria-endemic countries. However, global progress in malaria elimination has been hindered in recent years, with the annual number of cases reaching 249 million in 2022 [1]. This slowing of progress has been attributed in part to changes in mosquito behaviour and the spread of insecticide resistance, both of which could further threaten future progress by reducing the effectiveness of vector control measures. For instance, diurnal and outdoor biting can contribute to a substantial fraction of overall transmission [2, 3], and resistance to public health insecticides including pyrethroids, organochlorines, carbamates and organophosphates is widespread in sub-Saharan Africa [1]. As a result, there is increasing interest in the use of larval source management (LSM) to supplement current vector control interventions, especially in settings of moderate to low transmission and in high transmission settings with high rates of insecticide resistance or outdoor biting [4].

LSM interventions could be especially well-suited for certain settings in sub-Saharan Africa, a region that accounts for over 90% of malaria cases globally [1]. LSM interventions are particularly feasible and cost-effective in settings where habitats are 'few, fixed and findable' according to the World Health Organization (WHO), which recommends environmental management (i.e. habitat modification and manipulation) as the primary LSM intervention whenever possible, and the regular application of biological or chemical larvicides in habitats that cannot be removed or modified [4]. In particular, there has been an important focus on LSM interventions targeting rice fields, where the use of larvicides, the introduction of fish and intermittent irrigation practices have all proven to be effective in reducing larval abundance [5, 6]. Demand for rice has surged in Africa in recent decades, and the area of cultivated rice has more than doubled in the last 20 years [7]. Aquatic conditions in rice fields are particularly favourable to the development of some of the most important malaria vectors in Africa, such as *Anopheles funestus* and the species complex *Anopheles gambiae* [8], and the abundance of adult mosquitoes is often higher near rice-growing areas [5]. A recent meta-analysis focused on the past two decades found that rice-growing communities in Africa have experienced significantly higher malaria prevalence levels than communities that do not grow rice [9], further evidence for the importance of these water bodies as larval habitat. However, for LSM interventions to target rice fields and other larval habitats, their implementation requires an accurate characterization of these larval habitats to ensure interventions are well-placed and well-timed [4, 10].

Rice cultivation occurs mainly during the period of water abundance, generally associated with the rainy season, which favours mosquito larval development and coincides with a period of highest malaria transmission [9]. The early, pre-reproductive stages of rice fields provide ideal ecological conditions for *An. gambiae* larvae, which prefer fresh, oxygenated, calm, clear water 2–10 cm deep and silty or clay soils [11–13]. LSM techniques that target these time periods to apply larvicide have shown success in reducing mosquito populations. While context specific, previous research has identified the optimal frequency for the application of the biolarvicide *Bacillus thuringiensis israelensis* (*Bti*) to rice fields [14] and the ideal climatic conditions for *Bti* application [9], in some cases reducing larval densities by up to 95% [15]. In addition, the effectiveness of LSM in rice fields was demonstrated in Madagascar, where they halved the number of mosquito larvae in rice fields by applying Bti twice per month over a 2 month period from February to July 2022, during the rainy season [16]. Optimizing LSM programmes by targeting actively flooded rice fields and identifying those at their pre-productive (e.g. early flooding) stage could help low-resourced vector control programmes better allocate their efforts. Remote flood mapping of rice fields is one such way to provide necessary information to accurately identify active rice fields and their water coverage.

The use of remote sensing for the environmental monitoring of rice fields and water surfaces is increasingly common in agriculture and vector surveillance thanks to the growing availability of data from earth observation satellites and drones [17]. One technique consists of generating spectral indices from optical satellites with relatively high spatio-temporal resolution (e.g. Sentinel-2, LandSat, MODIS), but these indices require field validation to be sufficiently accurate [18, 19]. In addition, the quality and availability of optical images depends on cloud cover, which can have a major impact on the signal and, therefore, on the number of usable images, especially in humid tropical areas during rainy seasons, where malaria transmission is often highest. Drones can generate spatial information at high resolutions (under 10 cm) and at temporal intervals determined by the user, and can be of particular interest in settings already using drones for LSM interventions (e.g. application of larvicides) [20–23]. Unfortunately, in addition to implementation barriers such as community acceptance, national regulations and costs, drones can only cover small areas, which prevents their routine use at scale [22].

Synthetic aperture radar (SAR) data are better suited to detect changes in surface water over large geographic areas regardless of weather and light conditions [24, 25]. However, the resolution of freely available SAR data from Sentinel-1 satellites can be insufficient to detect small larval habitats and to correctly classify particular land cover features of interest, such as rice fields [22, 25]. To build decision making tools that can enable and guide the widespread implementation of LSM interventions targeting larval habitats in rice fields over larger areas (such as districts or provinces), complementary approaches are needed for larval habitat monitoring that leverage imagery at very high spatial resolution for larval habitat identification and SAR data for temporal monitoring of flooding dynamics.

The goal of this study was to develop and validate a method that allows for the longitudinal monitoring of flooding dynamics in individual rice fields over very large geographic areas relevant to national malaria control programmes aiming to implement LSM at scale. This was demonstrated for a 3971 km^2 malaria-endemic district in Madagascar, a major rice producing country where malaria incidence is increasing and where LSM interventions targeting rice fields are being piloted [16]. A field-validated classification model was applied to radar imagery to characterize rice field dynamics from 2016 to 2022 for over 17,000 rice fields. These dynamics were summarized into indicators representing seasonality and made available via an online application. Because the optimal conditions within larval habitats and thus the specific characteristics of LSM programme design are context-specific, this study focused on creating a flexible tool that provides key information on rice field flooding dynamics that can inform a wide range of programme designs and priorities in a variety of settings, rather than fine-tuning the tool in the study area with entomological or epidemiological data. Scale-up of these methods could enable wider implementation of evidence-based LSM interventions and reduce malaria burdens in contexts where irrigated agriculture is a major transmission driver.

Methods

Study area

This study was conducted in Ifanadiana, a rural district located in the Vatovavy region of southeastern Madagascar. The district covers an area of approximately 3970 km^2, receives an annual precipitation of 1200 mm, and has a humid tropical climate and a population of approximately 200,000 inhabitants [26]. The district consists of 15 communes (administrative units with an average of 13,000 inhabitants) and 195 fokontany (local administrative units consisting of several villages with an average of about 1,000 inhabitants) [27]. Ifanadiana is characterized by its geographical diversity, including mountains, valleys with water sources, rivers and dense, very humid vegetation ideal for agriculture. The district is predominantly rural, with an economy dominated by agriculture, primarily rice cultivation [28]. Rice cultivation practices in the district vary according to the geographical context, resulting in a diversity of cultivation seasons. Some farmers plant rice once a year, while others plant rice twice a year. This variation is influenced by irrigation availability and access to water, critical factors for understanding how seasonal differences contribute to the diversity in the spatio-temporal dynamics of rice field flooding across the district.

Ifanadiana district is malaria endemic, with an estimated annual incidence of approximately 500 cases per 1000 inhabitants after accounting for underreporting and prevalence rates as high as 80% during the malaria season [29]. The district exhibits seasonal transmission dynamics linked to climatic patterns, with a low transmission season between June and November and a high transmission season between December and May. Previous studies have shown that rice fields favour malaria transmission, in combination with other climatic and socioeconomic factors in the district [30]. Therefore, this study aimed to understand the flooding dynamics of all rice fields in the district in order to contribute to precise and targeted malaria control efforts.

Identification of rice field flooding thresholds using field data and Sentinel-1 images

Monitoring the spatio-temporal dynamics of rice field flooding was based on three fundamental steps: field data collection, downloading data to extract pixel values from SAR imagery using Google Earth Engine (GEE) for analysis processing, and determination of optimal thresholds to classify different water classes (Fig. 1). First, field observations were conducted to obtain temporal and spatial representativity of rice field flooding dynamics (Fig. 2). A temporal sampling campaign was conducted monthly on 7 rice fields between February 2021 and February 2022 (Table 1). A spatial sampling campaign was conducted in the dry season (October 17–21, 2022) and the rainy season (February 27–March 3, 2023), covering 54 rice fields in the district (Table 1). These visits, conducted by a team of 5 people, aimed to collect representative samples of three categories of flooding dynamics ("open water", "vegetated water", and "no water"), and to collect information on rice plant height, water depth, rice field characteristics, observation landmarks and their orientation, and observed water class types. NextGIS Mobile (version 2.6.49) was used to geolocate each rice field and store information and photos directly in the attributes of the geographic features [31]. These data

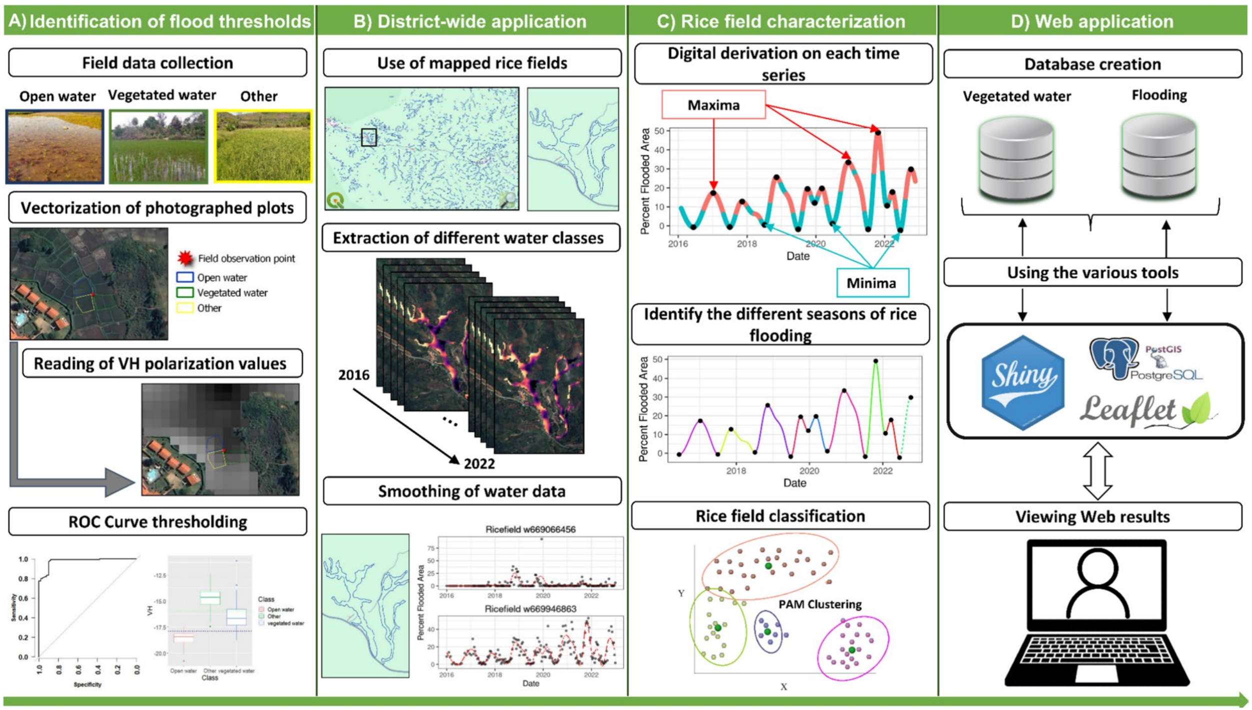

Fig. 1 Steps in the characterization of individual rice field dynamics at large spatial scales for operational use in malaria control. **a** Training of classification models to classify three flooding classes using radar imagery based on field-collected data. **b** District-wide application of classification models to all rice fields in the district and smoothing of resulting time series. **c** Estimation of temporal indicators for each rice field and grouping of rice fields based on flooding dynamics. **d** Integration of resulting rice field and fokontany-level information into an openly available web application

allowed the manual classification of pixels in each rice field that corresponded to the three water class categories used to train the classification model.

Second, SAR satellite data were obtained on these field-monitored rice fields. This technology is particularly suitable for monitoring the spatio-temporal dynamics of flooding in rice fields due to its ability to penetrate clouds which are numerous in tropical mountainous areas and operate day and night [32, 33]. Among the different polarizations used by SARs, the VH (Vertical transmit and Horizontal receive) polarization of Sentinel-1 C-band imagery is particularly relevant for detecting open water (low backscatter) from areas covered by emerging vegetation and also young rice fields (double bounce, high backscatter) [34]. Sentinel-1 SAR data from descending orbits at the ARD (Analysis Ready Data) level available on the GEE platform were used in this study [35]. These data have already undergone the following preprocessing steps: orbital corrections for precise localization, radiometric corrections to convert raw values into usable backscatter coefficients and remove noise effects, and terrain geocoding to project images onto a cartographic grid that accounts for topography and accurately represents ground geometry.

Third, using data collected in the previous two phases, optimal thresholds of VH polarization values were determined to distinguish between the three categories of flooding: "open water", "vegetated water", and "no water". These categories allow for differentiation between flooded areas and periods with and without productive agriculture, to better target the open-water and early flooding season most associated with malaria incidence in this study area [36]. The approach began with data preparation, including georeferencing and vectorizing observed plots as shapefiles, where each plot corresponded to an observation point containing a water class based on field observations (Fig. 1a). Sentinel-1 imagery acquired on the date closest to the field visits (range of 0–14 days difference) was then processed, identifying pixels corresponding to each plot and extracting VH polarization values for each field-collected water class. Receiver Operating Characteristic (ROC) curves were used to identify the best discriminative thresholds between the two classes. ROC curves perform well at two-class discrimination by identifying the optimal threshold that maximizes the sensitivity and specificity rates, while remaining relatively simple and resource efficient to implement at scale. ROC

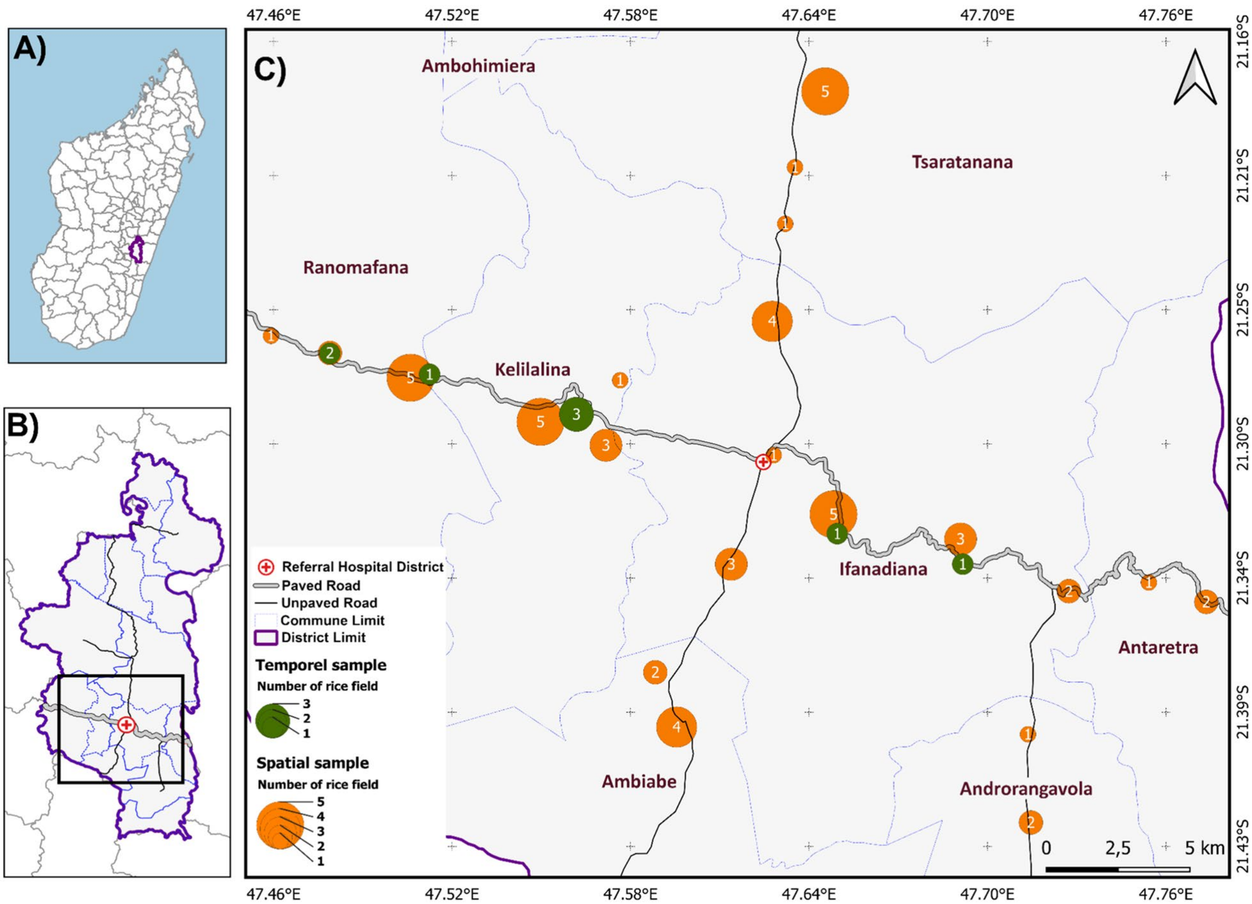

Fig. 2 Map of the study area showing the location of the data collected in the field for the temporal and spatial sampling. **a** Map of Madagascar. **b** Map of district Ifanadiana with delimited box corresponding to panel C. **c** Location of temporal and spatial samples of flooding dynamics collected in the field

Table 1 Number of field observations used to train the classification model

	Number of rice fields	No. observation points (photos)	No. polygons
Temporal sample			
Monthly (February 2021–February 2022)	7	63	89
Spatial sample			
Dry season (October 17 2022–October 21 2022)	54	203	222
Wet season (27 February 2023–02 March 2023)	54	181	204

curves were used to identify thresholds from training data already classified between two classes: one to discriminate "open water" from "vegetated water", and another to discriminate "vegetated water" from "no water". To ensure robustness and generalizability of the thresholds, the data were spatially stratified, with data around the EAST–WEST axis used as training data (77%) and those from the NORTH–SOUTH axis (23%) used as validation data. This approach allowed for the calculation of the sensitivity and specificity for each threshold (Fig. 3).

Estimation of individual rice field flooding dynamics in Ifanadiana district

The classification models and thresholds obtained from field data were applied to SAR imagery corresponding to all rice fields within the district from January 2016 to December 2022 (Fig. 1b). To do so, all of the

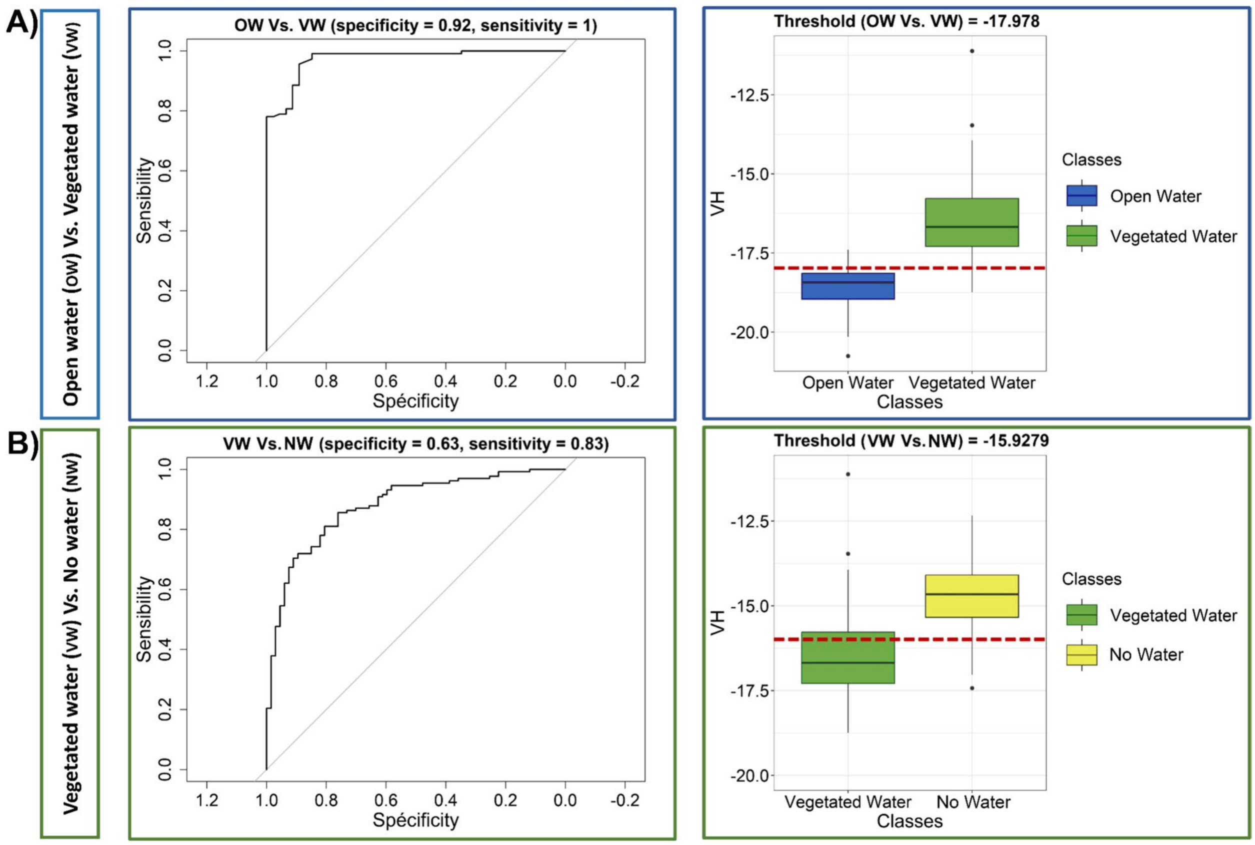

Fig. 3 Result of receiver operating characteristic (ROC) curve analyses on the test dataset and resulting threshold in VH polarizations. **a** Comparison of ROC Curve between Open water (Positive) and Vegetated water (Negative) of sample rice fields. **b** Comparison of ROC Curve between Vegetated water (Positive) and No water (Negative) of sample rice fields. Both ROC curve confusion matrices are described in the Results section and (see Additional File 1: Tables S1–S3)

rice fields, buildings, and administrative boundaries in the district were first identified via a participatory mapping exercise on the OpenStreetMap (OSM) platform in 2019. Full details of this mapping exercise are reported in [37]. This data was downloaded using the QGIS QuickOSM extension [38] [August 23 2023], obtaining the boundaries of 17,321 rice fields and over 100,000 buildings. The administrative boundaries of the district's 15 communes and 195 fokontany were also obtained [39], as well as precipitation data for the duration of the study from Africa Rainfall Climate 2 [40], which was used to calculate the daily precipitation average for the district.

Sentinel-1 images collected every 12 days from January 01 2016–December 23 2022, were used at the same ARD processing level as described above. For each Sentinel-1 image, pixels located fully-within the rice fields mapped on OSM were filtered and classified into the same three water categories by applying the optimal thresholds determined by the classification model. Finally, the areas and proportions of coverage of each water class in each rice field were calculated for each acquisition date of the available Sentinel-1 images.

SAR imagery is impacted by speckle noise, which can be caused by backscatter from pixels with heterogeneous surfaces [41]. This noise is particularly problematic in time series analysis when attempting to identify local minima and maxima. Temporal smoothing was therefore applied to the resulting time series to reduce the influence of stochastic noise (Fig. 1b). For each rice field, four smoothing techniques were compared: cubic-spline, polynomial, basis-spline, and natural spline. For cubic-spline, basis-spline, and natural-spline techniques, the degrees of freedom were limited to 4 per year, to allow the smooths to fit the seasonality of the data without overfitting to short-term trends. For the polynomial technique, the degrees of freedom were reduced to 2 per year due to convergence issues at higher values. For each rice field, the smoothing technique that resulted in the lowest residual sum of squares was chosen via leave-one-out cross validation, and resulting model was used to create a weekly time series for that rice field (see Additional File 1:

Table S4). The smoothing method was applied separately to the vegetated water class and the sum of both flooded water classes (vegetated + open water), referred to as total flooded area.

Individual rice field characterization and estimation of aggregate indicators

An algorithm was developed to create summary statistics regarding the agricultural season from each rice field's smoothed time series of flooded areas (Fig. 1c). First, numerical derivation was performed on each time series to identify local minima and maxima values of the area of each class using a central derivation across a time difference of 1 day. Each local minima or maxima was then assessed to determine whether it represented the beginning, peak, or end of an agricultural season. Local minima and maxima were chosen to delineate the beginning and end of a flooding season to ensure that the seasons included the beginning of larval habitat flooding, when larvicide is most effective [42]. The beginning of a season corresponded to a local minimum that was followed by a maximum that occurred at a flooding value at least 10% of the maximum flooding value of that rice field higher than the focal minimum. The peak of a season corresponded to a local maximum that occurred at a flooding value of at least 10% of the maximum flooding value of that rice field higher than the nearest minimum on either side of the focal maximum. Maxima that did not meet this threshold were defined as intra-season maxima. The end of a season corresponded to a minimum that had a maximum between it and the following minimum that occurred at a flooding value of at least 10% of the maximum flooding value. If the threshold was not met, the period between the two minima was classified as inactive. This resulted in the definition of a season being the period between two minima with a maximum at least 10% higher than the surrounding minima (see Additional File 1: Figs. S1–S3). From the identified beginnings, peaks, and ends of seasons, the following statistics were estimated for each agricultural season and rice field: start date, end date, minimum flooding value, maximum flooding value, date of maximum flooding, and whether the season was inactive (no flooding). These statistics were then summarized to rice-field level statistics over the seven year time period.

To provide useful information to operational programmes that implement LSM interventions, individual rice field data need to be aggregated in a way that can help with the design, site prioritization, and follow-up of interventions. Data were aggregated in two ways. First, to visualize spatial trends in these indicators, the average of each statistic was obtained per fokontany (smallest administrative unit) to be displayed in corresponding maps. Second, a semi-supervised time-series classification algorithm was applied to categorize rice field flooding dynamics into a limited set of homogeneous groups. For this, rice fields that remained less than 20% flooded during the study period or were inactive for more than 50% the study period were manually classified as inactive. The remaining rice fields (N = 14,693) were then classified into groups with similar time series characteristics by applying an algorithmic methodology based on dynamic time warping (DTW) and partitioning around the median (PAM) to the time series, adapting an approach used by Legendre et al. for the clustering of malaria time-series [43–45]. The approach consists of two distinct steps: calculating a metric of distance between all pairs of smoothed rice field time series using DTW, and clustering of the smoothed time series using the PAM algorithm applied to the DTW distance matrix. DTW is a method that measures the similarity between two time-series based on their amplitude and phases [46]. The determination of the optimal number of clusters was based on the ratio between the inter- and intra-group variance of the rice fields (see Additional File 1: Fig. S4), using the index quality measure of Calinski-Harabasz [47]. This resulted in a seven-category classification for the rice field dataset, with descriptive names assigned based on their average dynamics: inactive before mid-year 2018 and low flood coverage, low flood coverage, low and moderate flood coverage, moderate flood coverage, moderate flood coverage with two seasons per year, high flood coverage, and very high flood coverage. For this classification, the package "parallelDist", version 0.2.6 [48], was used for implementing the DTW calculations and "parallelpam", version 1.4 [49], was used for clustering via PAM, both of which offer the ability to run calculations in parallel to speed up the processing. All analyses were done in R software, version 4.3. Finally, determining the population at risk from a particular larval habitat is an important factor to consider for site prioritization of LSM interventions. The number of buildings within a 500 m radius representing the average flight range of *Anopheles* mosquitoes (*funestus* and *gambiae*) [50], was estimated around each rice field as a proxy for population at risk from that rice field (i.e., residents exposed to mosquitoes) [51], using OSM spatial data on rice fields and households. From this, rice fields were classified into two categories: those with less than 50 surrounding buildings and those with 50 or more surrounding buildings.

Integration of rice field monitoring indicators into an e-health tool

To demonstrate how rice field monitoring can be used for operational purposes during LSM implementation, all the data and results obtained, including the location and temporal dynamics of rice fields, were integrated into a web application developed with the "R Shiny" platform (Fig. 1d). The application allows for the visualization of key information at the district, fokontany, and individual rice field levels. This approach aims to facilitate the use and interpretation of results, while ensuring interoperability of information to support programmatic teams involved in mosquito larvae surveillance and control. Spatial junction techniques were performed with administrative boundaries to create complete geographic profiles for each fokontany and rice field. To implement the application, PostgreSQL was used for the spatial database management system (DBMS) with the "PostGIS" extension, as well as the R packages "leaflet", version 2.2.2 [52] for cartographic visualization and "Rpostgres", version 1.4.7 [53] and "rpostgis", version 1.5.1 [53] for connection to the DBMS and manipulation of geographic data.

Results

Analyses of the optimal threshold in Sentinel-1 SAR images for each water class of interest using field data resulted in a classification where VH polarization values below -17.98 dB were considered open water, those between − 17.98 and − 15.93 dB as vegetated water, and those above − 15.93 dB as no water (Fig. 3). The classification model of open water and vegetated water had a sensitivity (i.e. identification of vegetated water) of 1 and a specificity (i.e. identification of open water) of 0.92 with a precision of 0.88 and F1 scores of 0.94 (Fig. 3 and see Additional File 1: Table S1) when applied to the testing dataset. The classification error matrix shows 19 false positives out of 161 misclassified as vegetated water and no false negative for the open water class (see Additional File 1: Table S2). The classification model of vegetated water and no water classes had a sensitivity (i.e. identification of vegetated water) of 0.83 and a specificity (i.e. identification of no water) of 0.63 with a precision of 0.80 and F1 scores of 0.81 (Fig. 3 and see Additional File 1: Table S1) when applied to the testing dataset. The classification error matrix shows 50 false positives out of 248 misclassified as no water and 40 false negatives out of 125 misclassified as vegetated water class (see Additional File 1: Table S3).

After applying these thresholds to the 16,982 rice fields in Ifanadiana District and analyzing the resulting time-series of total flood coverage (open water and vegetated water combined), rice fields were identified as having either one or two distinct flooding seasons during each agricultural year (Table 2), the timing of which varied considerably within the district (Fig. 4). The median percentage of water coverage in rice fields at the peak of the flooding season was 43% (IQR 29–58%) (Table 2). All rice fields had at least one "primary" flooding season, which began in July and attained its peak flooding in

Table 2 Summary statistics of temporal rice field flooding dynamics for 16,982 rice fields

Description	Mode	Median	IQR (25–75%)	Min–Max
Full time period (6 agricultural years, N = 16,982)				
Number of seasons	6	6	6–7	1–11
Number of agricultural years with more than one season	0	0	0–1	0–5
Number of inactive seasons	0	1	0–1	0–5
Maximum percentage of flooded area	35	43	29–58	0–100
Primary season (N = 16,982)				
Beginning of season (month of year)[a]	6	5	4–6	1–12
End of season (month of year)[a]	6	5	2–6	1–12
Month of highest percentage of flooded area[a]	10	10	9–10	1–12
Median length of season (days)	370	336	294–363	145–1546
Average change in percentage of flooded area during the season (maximum flooded percentage—minimum flooded percentage)	19	22	16–31	0–86
Secondary season (N = 5644)				
Beginning of season (month of year)[a]	12	3	1–12	1–12
End of season (month of year)[a]	6	6	6–7	1–12
Month of highest percentage of flooded area[a]	3	3	3–4	1–12
Median length of season (days)	160	177	160–202	104–588
Average change in percentage of flooded area during the season (maximum flooded percentage–minimum flooded percentage)	7	15	9–24	0–99

Statistics were calculated for each rice field across the 6 year agricultural period (July 01 2016–June 30 2022). Summary statistics represent the summary across the full dataset of rice fields

[a] Each rice field was assigned the mode of the beginning month of each season across the 6 year time period

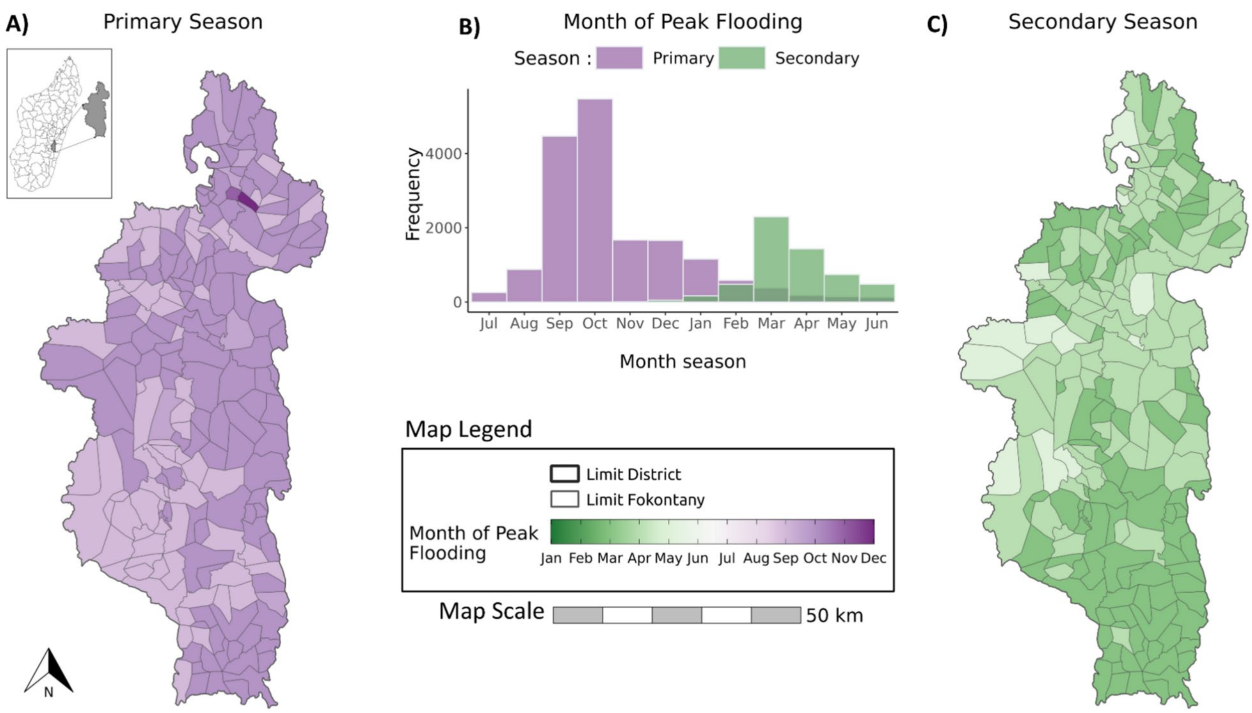

Fig. 4 Spatial distribution of the timing of peak flooding in rice fields in Ifanadiana. **a** Month of peak flooding during the primary flooding season. **b** Histogram of the timing of peak flooding for the primary and secondary flooding seasons in the 16,982 rice fields. **c** Month of peak flooding during the secondary flooding season. A similar figure is available with vegetated water results only (see Additional File 1: Figure S5)

September–October (58.53%), before the peak in precipitation (Figs. 4b, 5b). The median duration of the primary flooding season was 336 days (IQR 294–363 days), with a mode exceeding one year (Table 2). These rice fields did not remain at high flood coverage during the full extent of this time, but rather had strong annual seasonality, with minimum flooding at the beginning and end of the season (Fig. 5). Rice fields typically experienced two flood phases per year, and some remained flooded after cultivation in the absence of drainage systems (Fig. 5). Flood coverage increased by 22% of the total field area (IQR 16–31%) between the beginning of a season and the moment of peak flooding (Table 2). The spatial distribution showed that rice fields in low-lying fokontany (on the eastern side of the district) were flooded later than those at higher elevation (Fig. 4a). One third of the district's rice fields (N = 5644) remained flooded during a secondary rice growing season at least once during the study period. The majority of these rice fields (66.03%) experienced the peak flooding of their second season between March and April. The secondary flooding season had a shorter duration than the primary season, with a median of 177 days (IQR 160–202 days) (Table 2). The spatial distribution shows that rice fields in the southern and northern parts of the district flood earlier in the secondary season than in the rest of the district (Fig. 4c). During the 6-year study period, 37.90% of rice fields had at least one inactive season, where the increase in flood coverage was below 10%. Similar results are available when considering only the vegetated water data class (see Additional File 1: Figure S5 and Table S5 and S7).

Classification of rice fields according to their flood dynamics

Using the DTW classification algorithm, an optimum of eight groups of rice fields with similar flooding dynamics was obtained (Table 3, Fig. 5a). The classification of these rice fields showed that 28.79% had high flood coverage (high flood coverage and very high flood coverage classes), 38.84% had moderate flood coverage (low to moderate flood coverage, moderate flood coverage, and moderate flood coverage with two seasons per year classes), 18.89% had low flood coverage (low flood coverage, and inactive before mid-year 2018 with low flood coverage classes), and the rest were always inactive (i.e., below 20% flood coverage) (Table 4). These classes showed similar seasonal patterns, but differed in the overall amount of flooded area of each rice field, with the exception of the always inactive rice fields, which were very flat with little flooded area, and the class of moderately flooded rice fields with two flood seasons per year (Fig. 5a and Table 4). Rainfall temporal patterns

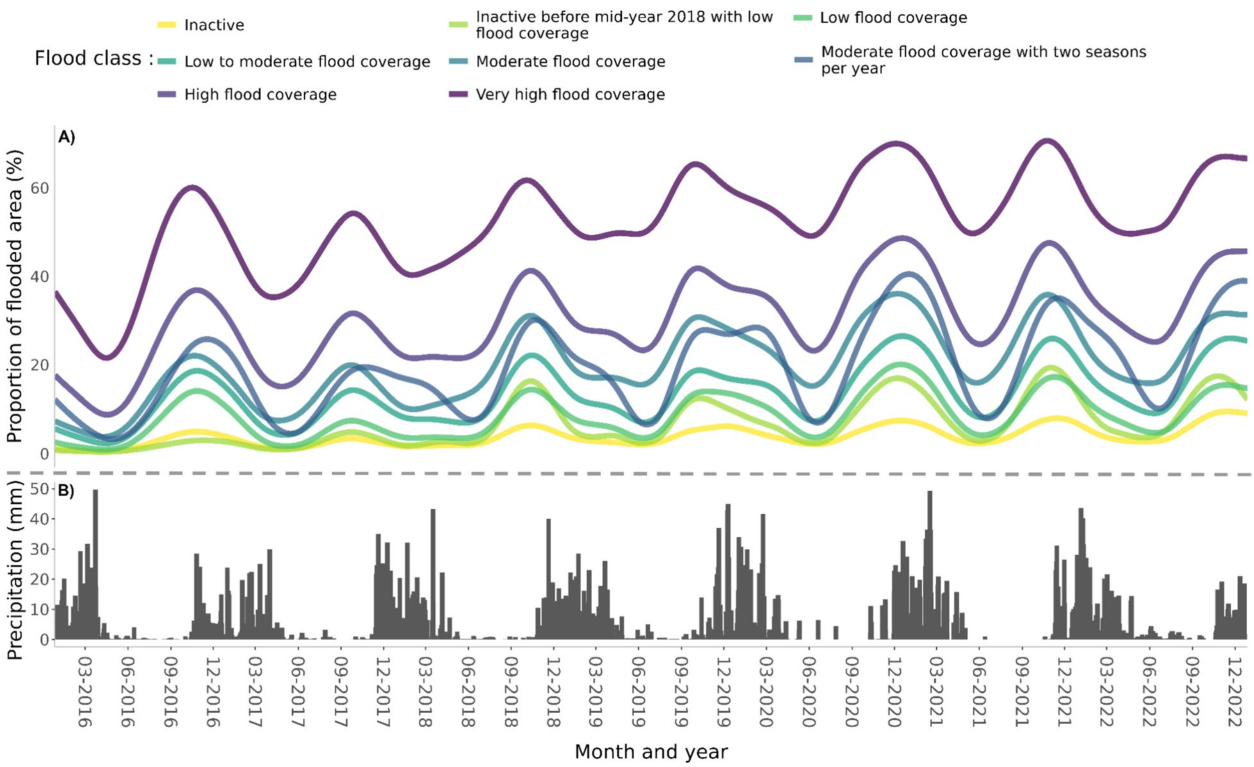

Fig. 5 Flooding dynamics from January 2016 to December 2022 by rice field class, Ifanadiana District. **a** Median time series of flooding dynamics for rice fields classified in the same group, with one colour per class. **b** Time series of weekly average precipitation in Ifanadiana District. More details on the range of rice field dynamics by flood class are available in Additional File 1: Fig. S6. A similar figure is available with results only for vegetated water (see Additional File 1: Fig. S7)

Table 3 Distribution of 16,982 supervised rice fields by the number of nearby households (within a 500 m radius) and time series classification group

Time series	Number of household < 50		Number of household ≥ 50	
	Number	Total area (Ha)	Number	Total area (Ha)
Inactive	1939 (11.42%)	872	350 (2.06%)	163
Inactive before mid-year 2018 with low flood coverage	804 (4.73%)	188	207 (1.22%)	66
Low flood coverage	1748 (10.30%)	884	449 (2.64%)	325
Low to moderate flood coverage	2095 (12.34%)	1817	542 (3.20%)	794
Moderate flood coverage	1715 (10.10%)	1165	337 (1.98%)	276
Moderate flood coverage with two seasons per year	1490 (8.77%)	2609	416 (2.45%)	997
High flood coverage	2776 (16.35%)	2107	474 (2.79%)	507
Very high flood coverage	1410 (8.30%)	436	230 (1.35%)	58

Similar information is available for the vegetated water flooding category alone (see Additional File 1: Table S6)

also followed these trends, but with a substantial lag in relation to the flooding dynamics, whereby the onset and peak of flooding typically occured several weeks before those of precipitation (Fig. 5). When the different rice field classes were combined with the number of households surrounding each rice field, results showed that the vast majority of rice fields (82.30%) were surrounded by fewer than 50 households, including nearly 25% of those that had high or very high flood coverage (Table 3). Only 17.7% of rice fields were surrounded by 50 or more households, including less than 5% of those with high or very high flood coverage (Table 3).

Table 4 Descriptive statistics of rice fields by flood season and time series class

Flood class (IQR: 25–75%)								
Description	**Inactive (N = 2289)**	**Inactive before mid-year 2018 with low flood coverage (N = 1011)**	**Low flood coverage (N = 2197)**	**Low to moderate flood coverage (N = 2637)**	**Moderate flood coverage (N = 2052)**	**Moderate flood coverage with two seasons per year (N = 1,906)**	**High flood coverage (N = 3,250)**	**Very high flood coverage (N = 1,640)**
Full time period (6 agricultural years)								
Number of seasons	6 (5–7)	7 (6–8)	6 (6–7)	6 (6–8)	6 (6–7)	6 (5–8)	6 (6–7)	6 (6–7)
Number of agricultural years with more than one season	0 (0–1)	0 (0–1)	0 (0–1)	0 (0–1)	0 (0–1)	0 (0–1)	0 (0–1)	0 (0–1)
Number of inactive seasons	1 (1–2)	1 (1–2)	1 (0–2)	1 (0–1)	1 (0–1)	0 (0–1)	1 (0–1)	1 (0–1)
Maximum percentage of flooded area	14 (10–17)	30 (25–39)	29 (24–37)	35 (30–42)	45 (38–53)	49 (42–57)	58 (51–66)	79 (71–87)
Primary season (N = 16,982)								
Beginning of season (month of year)[a]	5 (4–6)	6 (4–6)	5 (4–6)	5 (4–6)	5 (4–6)	6 (5–6)	5 (4–6)	4 (3–6)
End of season (month of year)[a]	5 (3–6)	4 (2–6)	5 (3–6)	5 (2–6)	4 (2–6)	6 (5–6)	5 (2–6)	3 (2–5)
Month of highest percentage of flooded area[a]	9 (8–10)	10 (9–10)	10 (9–10)	10 (9–10)	10 (9–10)	10 (3–10)	10 (9–10)	9 (9–10)
Median length of season (days)	322 (282–356)	307 (258–349)	336 (296–363)	339 (294–363)	342 (307–363)	349 (289–366)	342 (301–364)	341 (308–363)
Average change in percentage of flooded area during the season (maximum flooded percentage—minimum flooded percentage)	8 (6–11)	19 (15–24)	17 (14–22)	21 (17–26)	24 (19–30)	31 (25–39)	29 (22–37)	30 (24–37)
Secondary season (N = 5644)								
Beginning of season (month of year)[a]	3 (1–12)	2 (1–12)	2.5 (1–12)	3 (1–12)	2 (1–12)	11 (1–12)	10 (1–12)	10 (1–12)
End of season (month of year)[a]	7 (6–8)	6 (6–7)	6 (6–7)	6 (6–7)	6 (6–7)	6 (6–6)	6 (6–7)	6 (6–7)
Month of highest percentage of flooded area[a]	4 (3–5)	4 (3–4)	3 (3–4)	3 (3–4)	4 (3–4)	3 (3–4)	3 (3–4)	4 (3–5)

Table 4 (continued)

Flood class (IQR: 25–75%)								
Description	**Inactive (N = 2289)**	**Inactive before mid-year 2018 with low flood coverage (N = 1011)**	**Low flood coverage (N = 2197)**	**Low to moderate flood coverage (N = 2637)**	**Moderate flood coverage (N = 2052)**	**Moderate flood coverage with two seasons per year (N = 1,906)**	**High flood coverage (N = 3,250)**	**Very high flood coverage (N = 1,640)**
Median length of season (days)	188 (167–223)	168 (153–189)	175 (160–203)	175 (160–201)	174 (159–201)	175 (161–188)	175 (161–202)	189 (168–230)
Average change in percentage of flooded area during the season (maximum flooded percentage–minimum flooded percentage)	45 (3–8)	11 (7–16)	12 (8–17)	14 (9–20)	15 (10–22)	27 (18–36)	20 (13–30)	18 (12–28)

Results show the median and interquartile values (25% and 75%), for each indicator in the eight flooding classes over a period from July 01 2016 to June 30 2022 (6 agricultural years). Similar information is available for the vegetated water flooding category alone (see Additional File 1: Table S7)

[a] Each rice field was assigned the mode of the month of each season across the 6 year time period

E-health decision support tool for LSM interventions

The e-health tool was developed to help operational teams better prioritize, design, implement and monitor LSM interventions. The tool enables detailed monitoring of rice fields, with information on flooding dynamics to identify areas and periods that could present a higher risk to nearby residents. The application displays two measures of flooding (vegetated water and open water; vegetated water only) for spatio-temporal monitoring of rice field flooding via a filter bar (Fig. 6), with three spatial levels of information that can be useful for decision-making.

First, a visualization of the spatial distribution by fokontany is displayed to target areas of interest according to different indicators: the period of the flooding season (the beginning and end of the season, as well as the month of peak flooding), areas where rice fields are close to larger populations, and the type of rice field activity. Next, a user can select a specific fokontany to visualize rice fields by different colours according to their temporal flooding dynamics class, and view aggregated information for key indicators. Finally, the user can select an individual rice field to view the historical time series of its flooding dynamics and the location of nearby households (within 500 m).

Discussion

Current challenges in malaria control and elimination underscore the need to invest in new control strategies and corresponding decision support tools to guide their planning and implementation [1]. Mapping and monitoring of larval habitats, such as irrigated rice fields, is an essential prerequisite for the targeted deployment of larval source management (LSM) strategies. In this study, the precise identification of rice fields from OpenStreetMap (OSM) data was combined with Synthetic Aperture Radar (SAR) image analysis to track flooding dynamics in over 17,000 rice fields in rural Madagascar. From these time series, indicators relevant to the monitoring of rice field flooding dynamics for LSM interventions, such as the number and timing of agricultural seasons and a classification of rice fields according to the flooding level and temporal patterns and their proximity to human populations, were estimated. This information was demonstrated to be easily integrated into decision support tools to more effectively guide the planning and targeted implementation of LSM strategies via the accurate identification and monitoring of at-risk larval habitats.

This approach enables the classification and monitoring of rice fields at different levels of spatial aggregation (individual rice field, village, district) that are complementary in informing different phases and types of LSM interventions. For example, habitat modification strategies such as intermittent irrigation, drainage, or improved canals can help reduce mosquito breeding in land constantly flooded or with small fluctuations in water levels [4]. This method could aid in identifying rice fields with such characteristics based on historical flooding trends (e.g. less than one third of rice fields in Ifanadiana had

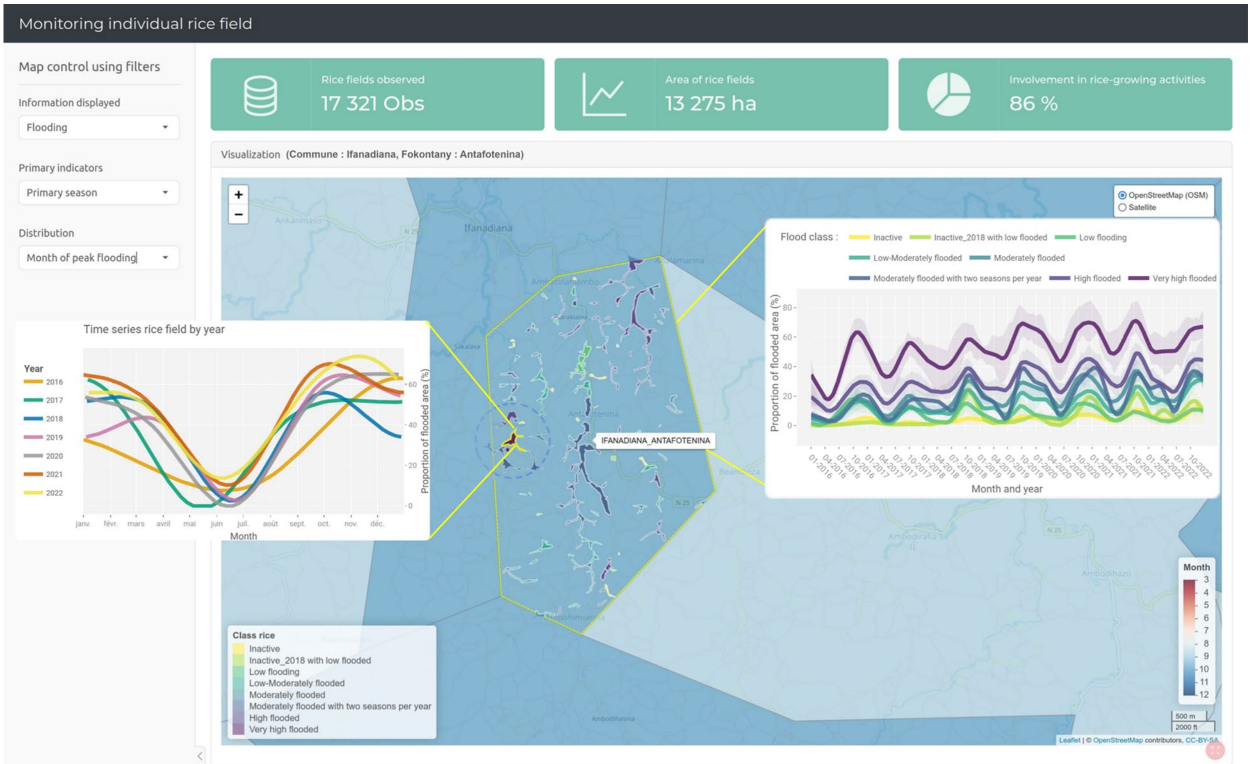

Fig. 6 Individual rice field monitoring tool to guide LSM interventions. Screenshot of the application showing the spatial distribution by fokontany of the month of peak flooding for the primary flooding season. The map in the center shows rice fields within a selected fokontany (limits in yellow) with colours according to flooding class. On the right, the time series of the different rice field classes are shown, aggregated within the fokontany (median and interquartile range). On the left, the time series per year of a selected rice field within the fokontany, with a 500 m radius in blue to delineate and visualize nearby households. The application is publicly available at https://lsm.pivot-dashboard.org/

high levels of flood coverage throughout the year), and evaluating prospectively whether the habitat modifications implemented have an impact on flooding patterns [54, 55]. Moreover, larvicide application requires frequent applications when the rice field is flooded in order to be effective [4]. In the planning phase, the results can help prioritize intervention sites based on historical flood dynamics, their size and proximity to populations, and identify key application periods. For instance, less than 5% of rice fields in Ifanadiana had high levels of flood coverage while being within 500 m of populations with 50 households or more. By monitoring flooding in selected rice fields in real time, programmes can adjust the frequency, duration, and stopping criteria for larvicide application to maximize their effectiveness while avoiding non-essential sites, thus optimizing the use of resources. Beyond its usefulness against malaria through LSM strategies, this approach could be useful in guiding surveillance and control interventions against other vector-borne diseases where rice fields play an important role in maintaining mosquito populations or could even contribute to improving food security and local agricultural development programmes, helping optimize rice cultivation practices to the flooding dynamics of individual rice fields [56].

The results show significant local heterogeneity in the number of flooding seasons, the timing of season onset, and the average level of flooding of rice fields. The average results are consistent with those from other global databases, such as RiceAtlas (thematic maps at a coarse spatial resolution and district scale by country), which show similar patterns of rice growing seasonality (incl. number of seasons, timing) as those estimated for Madagascar [57]. However, the estimated flooding seasons were about twice as long as the growing seasons estimated in RiceAtlas for Ifanadiana District, with some over a year long. This is likely due to the chosen method for seasonal delineation, which aims to identify the first increase in flood coverage, corresponding to the optimal period for larvicide application. Other methods, such as using a threshold percentage of flood coverage or a change in sign of the second derivative to delineate seasonal cutoffs, may be more appropriate for tracking agricultural production and result in shorter flooding seasons. This difference may also be due to the scale of analysis. Compared to other global estimates, this method provides an unprecedented level of detail on the spatio-temporal heterogeneity at the local level, such as the duration of flooding and rice cultivation, which varies according to the topography (high or low elevation) and the timing of their activities, making it possible to identify, for example, which villages within a district plant their rice later (Fig. 4) or which ones tend to have more than one cropping season. Taking this local heterogeneity into account may be key to the success of LSM strategies. Indeed, larval development varies considerably depending on conditions within individual rice fields, in combination with environmental and climatic conditions on a larger scale. For example, malaria vectors in Africa, such as *An. funestus* and *An. gambiae*, use stagnant surface water, such as aquatic agriculture, man-made ponds, drainage ditches, and natural ponds or rain pools, for larval habitat [51, 58]. In Madagascar, from the beginning of the dry season to the end of the rainy season, rice cultivation favours the development of mosquito larvae in rice fields [59] and is associated with an increase in the number of malaria cases caused by *An. gambiae* [51, 60]. In addition, the proximity of rice fields to households may increase the risk to the population, depending on the flight range and host preferences of *Anopheles* mosquitoes [61, 62]. About 17% of rice fields in Ifanadiana had more than 50 households within 500 m, and these parameters (i.e., population and distance thresholds) can be easily customized in order to guide site prioritization according to the local mosquito species, LSM programme budget and goals.

The innovation of this approach lies in the use of freely available SAR satellite imagery combined with OSM geographic data to track individual rice field flooding dynamics at a very large scale. The effectiveness of SAR imagery for mapping flooded vegetation has been validated by numerous studies using polarization VV/VH [63] and VH alone to detect open water [64, 65], some of which use artificial intelligence (AI) to determine thresholds for distinguishing water classes [66]. While such methods can offer improved classification accuracy, they are more complex to implement and require additional resources and expertise.

This study focused on implementing a simpler method that can be widely applicable for surveillance in rural areas of sub-Saharan Africa, by relying on field-collected, pre-classified data to train the model. This helped improve threshold accuracy through the application of ROC curves [67], allowing for a robust and reliable classification. Also, this approach is flexible and easily adaptable to other malaria endemic settings (Sentinel-1 data covers the whole globe), its main limitation being the availability of complete, high quality data on public platforms such as OpenStreetMap needed to locate the individual rice fields and residential areas [68]. Photo-interpretation mapping performed by humans, although resource intensive, can achieve remarkable accuracy, limit classification bias that is commonplace in AI-generated datasets, and help enrich public databases for other uses [69]. For example, through various initiatives, over 109,000 rice fields and 1,170,000 buildings have been mapped in seven districts of southeastern Madagascar, which may allow the approach to be scaled-up in several regions of Madagascar where malaria is highly endemic. Beyond Madagascar, parts of Africa and Asia are already relatively well mapped on OSM [68], demonstrating the potential of this approach for larger scales and diverse contexts. To circumvent the limitations of public data on rice fields, some studies have focused on using neural networks to identify favourable habitats for mosquitoes, such as rice fields, with benefits in terms of reduced financial and labor costs, although these methods are prone to error and rarely use very high-resolution data [70, 71]. An interesting alternative is the use of drone imagery, which provides much better resolution and can improve vector control activities. However, this approach is difficult to implement on scales required by malaria national control programmes due to regulatory constraints, high costs, safety challenges, community acceptance, and privacy concerns [22]. Therefore, drones are generally recommended for targeted ground surveys in small-scale pilot projects [21, 22, 72]. The approach proposed here represents a compromise between these two alternatives, allowing for the improvement of large-scale vector control interventions at a lower cost.

Despite the innovation and strengths in this approach, several limitations were identified. First, concurrent field surveys were not conducted to characterize larval productivity as a function of flood dynamics or to identify sites with high mosquito production [21]. In addition, other types of aquatic habitats besides rice fields which could also provide favourable conditions for the development of *An. funestus* larvae [73], were not considered. However, the link between local malaria dynamics in Ifanadiana and rice fields has been demonstrated previously [30, 36], and the proposed approach aims to guide LSM interventions that specifically target rice fields as priority larval habitats, as is the case in Madagascar [16]. Second, the spatial resolution of Sentinel-1 satellite data (10 m) limits the ability to robustly track small rice fields (< 0.04 ha), as the small number of pixels (some of which are partially outside the rice field) leads to greater stochasticity and uncertainty in the flooding results. In Ifanadiana, small rice fields represented only 13.48% of all rice fields in the district, but this could be an important limitation for the application of this method in contexts where small rice fields represent an important part of the larval habitat. Unfortunately, SAR imagery does not exist at finer resolutions than Sentinel-1, while simultaneously being freely available over such a wide area and regular passing frequency. Other SAR images, such as ALOS-2/PALSAR-2 L-band, offer less precise resolution (25 m), but are effective for identifying vegetated water areas and are rarely available [63]. The coarse resolution likely contributed to classification errors between vegetated water and no water classes. Such misclassification occurred when some pixels corresponded to vegetated crops without water, leading to errors in class assignment. This error affected only 24% of the samples misclassified into other categories, albeit with good classification accuracy (see Additional File 1: Table S3). Another source of uncertainty was the treatment of the time series, specifically the temporal smoothing. While temporal smoothing was necessary to reduce noise in the data, it may have also removed true short-term anomalies in the data, such as short-term flooding following high precipitation. Analyses were therefore limited to a frequency of 1-week or longer, at which these anomalies would have a smaller impact. Finally, the results of this study were integrated into a web-based decision support tool to demonstrate how it can effectively guide the local implementation of LSM interventions through a high-resolution, open-access, low-cost approach, but this study did not test the impact of the approach under real-world conditions of LSM intervention implementation. Operational research is needed to assess the usefulness of this approach in the field in close collaboration with programmatic teams.

Conclusion

While LSM strategies that target irrigated fields offer promising solutions for improving malaria control, there are currently few decision support tools for prioritizing and monitoring rice fields that would help optimize their design and implementation. This study presents an innovative and reproducible approach to monitor individual flooding dynamics in rice fields at large scales to guide LSM interventions, providing critical information at multiple levels of spatial aggregation that can be useful for decision making, such as the number of seasons, the exact flooding period, the level of flooding and activity. Scaling up this approach may facilitate broader adoption of evidence-based interventions using LSM, potentially decreasing malaria burdens in regions where rice fields are a significant contributor to larval habitat.

Abbreviations

ARD	Analysis ready data
Bti	Bacillus thuringiensis israelensis
DBMS	Spatial database management system
DTW	Dynamic time warping
IQR	Interquartile range
LSM	Larval source management
MODIS	Moderate resolution imaging spectroradiometer
OSM	OpenStreetMap
SAR	Synthetic aperture radar
VH	Vertical transmit and horizontal receive
WHO	World Health Organization

Supplementary Information

The online version contains supplementary material available at https://doi.org/10.1186/s12936-025-05344-3.

Additional file1 (DOCX 2261 KB)

Acknowledgements

We would like to thank Cathy NONINIRINA, Nadia RANOROARINALISOA, and Roger RIVOMANANA for their assistance with field data collection, and the Pivot Medical team for their work to improve health care in Ifanadiana District.

Author contributions

MR, TMR and AG conceived and designed the study. TC, CR, VH, FAI and ED used their expertise to validate the methodology and prepare the raw data for analysis. MR, TMR, AG, MVE and FAI analyzed the data. MR, TMR, AG and MVE contributed to the interpretation of the data and wrote the initial draft of the manuscript. All authors read, edited, and approved the final version of the manuscript.

Funding

This work was supported by a grant from Agence Nationale de la Recherche (Project SMALLER ANR-19-CE36-0001), with additional support from a grant from AfriCam project, funded by the French Development Agency (AFD) as part of PREACTS program and internal funding from Pivot.

Availability of data and materials

Data are available on OpenStreetMap (https://www.openstreetmap.org) and on the Shiny app (https://lsm.pivot-dashboard.org/). Analysis code is available on github (https://github.com/mvevans89/dynamique-riz.git) and Google Earth Engine (open water: https://code.earthengine.google.com/60e2941c1ee53a4ed55c52c281e387bf, vegetated water: https://code.earthengine.google.com/832f1a7284cc9ef6e68d4b1cf39212c7).

Declarations

Ethical approval and consent to participate

Not applicable.

Consent for publication

All authors approved the manuscript's submission for publication.

Competing interest

The authors declare no competing interests.

Author details

[1]ONG PIVOT, Ranomafana, Madagascar. [2]Institut de Recherche Pour Le Développement, UMR 224 MIVEGEC (IRD, UM, CNRS), Montpellier, France. [3]Université de Montpellier, ED 168 CBS2, Montpellier, France. [4]Department of Global Health and Social Medicine, Harvard Medical School, Boston, USA. [5]Espace Dev, IRD, Univ Montpellier, Univ Antilles, Univ Guyane, Univ Réunion, 5 Preah Monivong Blvd, Phnom Penh 12201, Cambodia. [6]Espace Dev, IRD, Univ Montpellier, Univ Antilles, Univ Guyane, Univ Réunion, Montpellier, France. [7]Espace-Dev, Univ La Réunion, Saint Denis, La Réunion, Cedex, France.

Received: 30 September 2024 Accepted: 22 March 2025
Published online: 01 April 2025

References

1. WHO. World malaria report 2023. Geneva: World Health Organization; 2023. Available from: https://cdn.who.int/media/docs/default-source/malaria/world-malaria-reports/world-malaria-report-2023.pdf
2. Sougoufara S, Ottih EC, Tripet F. The need for new vector control approaches targeting outdoor biting anopheline malaria vector communities. Parasit Vectors. 2020;13:295.
3. Sangbakembi-Ngounou C, Costantini C, Longo-Pendy NM, Ngoagouni C, Akone-Ella O, Rahola N, et al. Diurnal biting of malaria mosquitoes in the Central African Republic indicates residual transmission may be "out of control." Proc Natl Acad Sci USA. 2022;119: e2104282119.
4. WHO. Larval source management: a supplementary malaria vector control measure: an operational manual. Geneva: World Health Organization; 2013. Available from: https://iris.who.int/handle/10665/85379
5. Chan K, Bottomley C, Saito K, Lines J, Tusting LS. The control of malaria vectors in rice fields: a systematic review and meta-analysis. Sci Rep. 2022;12:19694.
6. Derua YA, Kweka EJ, Kisinza WN, Githeko AK, Mosha FW. Bacterial larvicides used for malaria vector control in sub-Saharan Africa: review of their effectiveness and operational feasibility. Parasit Vectors. 2019;12:426.
7. FAOSTAT. Food and Agriculture Organization of the United Nations. 2021. Available from: https://www.fao.org/faostat/en/#home
8. Lacey LA, Lacey CM. The medical importance of riceland mosquitoes and their control using alternatives to chemical insecticides. J Am Mosq Control Assoc Suppl. 1990;2:1–93.
9. Chan K, Tusting LS, Bottomley C, Saito K, Djouaka R, Lines J. Malaria transmission and prevalence in rice-growing versus non-rice-growing villages in Africa: a systematic review and meta-analysis. Lancet Planet Health. 2022;6:e257–69.
10. Fornace KM, Diaz AV, Lines J, Drakeley CJ. Achieving global malaria eradication in changing landscapes. Malar J. 2021;20:69.
11. Diuk-Wasser MA, Dolo G, Bagayoko M, Sogoba N, Toure MB, Moghaddam M, et al. Patterns of irrigated rice growth and malaria vector breeding in Mali using multi-temporal ERS-2 synthetic aperture radar. Int J Remote Sens. 2006;27:535–48.
12. Akpodiete NO, Tripet F. Laboratory and microcosm experiments reveal contrasted adaptive responses to ammonia and water mineralisation in aquatic stages of the sibling species *Anopheles gambiae* (sensu stricto) and *Anopheles coluzzii*. Parasit Vectors. 2021;14:17.
13. Hardy H, Hopkins R, Mnyone L, Hawkes FM. Manure and mosquitoes: life history traits of two malaria vector species enhanced by larval exposure to cow dung, whilst chicken dung has a strong negative effect. Parasit Vectors. 2022;15:472.
14. Mazigo HD, Mboera LEG, Rumisha SF, Kweka EJ. Malaria mosquito control in rice paddy farms using biolarvicide mixed with fertilizer in Tanzania: semi-field experiments. Malar J. 2019;18:226.
15. Fillinger U, Lindsay SW. Suppression of exposure to malaria vectors by an order of magnitude using microbial larvicides in rural Kenya. Trop Med Int Health. 2006;11:1629–42.
16. USAID/CDC. U. S. President's Malaria Initiative – Madagascar Malaria Operational Plan FY 2023. PMI. 2022. Available from: https://www.pmi.gov/where-we-work/madagascar/
17. Li L, Xin X, Zhao J, Yang A, Wu S, Zhang H, et al. Remote sensing monitoring and assessment of global vegetation status and changes during 2016–2020. Sensors. 2023;23:8452.
18. Luo C, Liu H, Fu Q, Guan H, Ye Q, Zhang X, et al. Mapping the fallowed area of paddy fields on Sanjiang Plain of Northeast China to assist water security assessments. J Integrat Agricult. 2020;19:1885–96.
19. Tornos L, Huesca M, Dominguez JA, Moyano MC, Cicuendez V, Recuero L, et al. Assessment of MODIS spectral indices for determining rice paddy agricultural practices and hydroperiod. ISPRS J Photogram Remote Sens. 2015;101:110–24.
20. Carrasco-Escobar G, Manrique E, Ruiz-Cabrejos J, Saavedra M, Alava F, Bickersmith S, et al. High-accuracy detection of malaria vector larval habitats using drone-based multispectral imagery. PLoS Negl Trop Dis. 2019;13: e0007105.
21. Byrne I, Aure W, Manin BO, Vythilingam I, Ferguson HM, Drakeley CJ, et al. Environmental and spatial risk factors for the larval habitats of *Plasmodium knowlesi* vectors in Sabah. Malaysian Borneo Sci Rep. 2021;11:11810.
22. Carrasco-Escobar G, Moreno M, Fornace K, Herrera-Varela M, Manrique E, Conn JE. The use of drones for mosquito surveillance and control. Parasit Vectors. 2022;15:473.
23. Trujillano F, Jimenez Garay G, Alatrista-Salas H, Byrne I, Nunez-del-Prado M, Chan K, et al. Mapping malaria vector habitats in West Africa: drone imagery and deep learning analysis for targeted vector surveillance. Remote Sens. 2023;15:2775.
24. Bayik C, Abdikan S, Ozbulak G, Alasag T, Aydemir S, Balik Sanli F. Exploiting multi-temporal sentinel-1 sar data for flood extend mapping. Int Arch Photogram Remote Sens Spatial Inform Sci. 2018;XLII-3-W4:109–13.
25. Catry T, Li Z, Roux E, Herbreteau V, Gurgel H, Mangeas M, et al. Wetlands and Malaria in the Amazon: guidelines for the use of synthetic aperture radar remote-sensing. IJERPH. 2018;15:468.
26. INSTAT 2020. Troisième recensement général de la population et de l'habitation (RGPH-3). 2020. Available from: https://www.instat.mg/documents/upload/main/INSTAT_RGPH3-Definitif-ResultatsGlogaux-Tome1_17-2021.pdf
27. Cordier LF, Kalaris K, Rakotonanahary RJL, Rakotonirina L, Haruna J, Mayfield A, et al. Networks of care in rural Madagascar for achieving universal health coverage in Ifanadiana District. Health Systems Reform. 2020;6: e1841437.
28. Miller AC, Ramananjato RH, Garchitorena A, Rabeza VR, Gikic D, Cripps A, et al. Baseline population health conditions ahead of a health system strengthening program in rural Madagascar. Glob Health Action. 2017;10:1329961.
29. Evans MV, Ihantamalala FA, Randriamihaja M, Aina AT, Bonds MH, Finnegan KE, et al. Applying a zero-corrected, gravity model estimator reduces bias due to heterogeneity in healthcare utilization in community-scale, passive surveillance datasets of endemic diseases. Sci Rep. 2023;13:21288.
30. Pourtois JD, Tallam K, Jones I, Hyde E, Chamberlin AJ, Evans MV, et al. Climatic, land-use and socio-economic factors can predict malaria dynamics at fine spatial scales relevant to local health actors: evidence from rural Madagascar. PLoS Glob Public Health. 2023;3: e0001607.
31. NextGIS Mobile. 2013. Available from: https://play.google.com/store/apps/details?id=com.nextgis.mobile
32. Fletcher K, Agency ES. Sentinel-1: ESA's Radar Observatory Mission for GMES Operational Services. ESA Communications; 2012. Available from: https://sentinel.esa.int/documents/247904/349449/S1_SP-1322_1.pdf
33. Zhan P, Zhu W, Li N. An automated rice mapping method based on flooding signals in synthetic aperture radar time series. Remote Sens Environ. 2021;252: 112112.
34. Nguyen DB, Gruber A, Wagner W. Mapping rice extent and cropping scheme in the Mekong Delta using Sentinel-1A data. Remote Sensing Letters. 2016;7:1209–18.
35. Mullissa A, Vollrath A, Odongo-Braun C, Slagter B, Balling J, Gou Y, et al. Sentinel-1 SAR Backscatter Analysis Ready Data Preparation in Google Earth Engine. Remote Sens. 2021;13:1954.
36. Evans MV, Ihantamalala FA, Randriamihaja M, Herbreteau V, Révillion C, Catry T, et al. Increasing the resolution of malaria early warning systems for use by local health actors. Malar J. 2025;24:30.
37. Ihantamalala FA, Herbreteau V, Révillion C, Randriamihaja M, Commins J, Andréambeloson T, et al. Improving geographical accessibility modeling for operational use by local health actors. Int J Health Geogr. 2020;19:1–15.
38. Herbreteau V, Révillion C, Trimaille E. GeoHealth and QuickOSM, Two QGIS plugins for health applications. In: Baghdadi N, Mallet C, Zribi M (eds.). QGIS and generic tools. 1st edn. Wiley; 2018. Available from: https://onlinelibrary.wiley.com/doi/https://doi.org/10.1002/9781119457091.ch7
39. OCHA. Madagascar - Subnational Administrative Boundaries. 2018. Available from: https://data.humdata.org/dataset/cod-ab-mdg
40. Novella NS, Thiaw WM. African rainfall climatology Version 2 for Famine Early Warning Systems. J Appl Meteorol Climatol. 2013;52:588–606.
41. Lee JS, Jurkevich L, Dewaele P, Wambacq P, Oosterlinck A. Speckle filtering of synthetic aperture radar images: a review. Remote Sens Rev. 1994;8:313–40.
42. Runge M, Mapua S, Nambunga I, Smith TA, Chitnis N, Okumu F, et al. Evaluation of different deployment strategies for larviciding to control malaria: a simulation study. Malar J. 2021;20:324.
43. Sardá-Espinosa A. Time-Series Clustering in R Using the dtwclust Package. The R Journal. 2019;11:22–43.

44. Montero P, Vilar JA. TSclust : An *R* Package for Time Series Clustering. J Stat Soft. 2014;62. Available from: http://www.jstatsoft.org/v62/i01/
45. Legendre E, Lehot L, Dieng S, Rebaudet S, Thu AM, Rae JD, et al. Malaria temporal dynamic clustering for surveillance and intervention planning. Epidemics. 2023;43: 100682.
46. Giorgino T. Computing and visualizing dynamic time warping alignments in R: The dtw Package. J Stat Softw. 2009;31:1–24.
47. Caliński T, Harabasz J. A dendrite method for cluster analysis. Commun Stat. 1974;3:1–27.
48. Eckert A, Godoy L, KS S. parallelDist: Parallel Distance Matrix Computation using Multiple Threads. 2022. Available from: https://cran.r-project.org/web/packages/parallelDist/index.html
49. Schubert E, Rousseeuw PJ. Fast and eager k-medoids clustering: O(k) runtime improvement of the PAM, CLARA, and CLARANS algorithms. Inf Syst. 2021;101:101804.
50. Verdonschot PFM, Besse-Lototskaya AA. Flight distance of mosquitoes (Culicidae): A metadata analysis to support the management of barrier zones around rewetted and newly constructed wetlands. Limnologica. 2014;45:69–79.
51. Arisco NJ, Rice BL, Tantely LM, Girod R, Emile GN, Randriamady HJ, et al. Variation in *Anopheles* distribution and predictors of malaria infection risk across regions of Madagascar. Malar J. 2020;19:348.
52. Cheng J, Schloerke B, Karambelkar B, Xie Y, Wickham H, Russell K, et al. leaflet: Create Interactive Web Maps with the JavaScript "Leaflet" Library. 2024. Available from: https://cran.r-project.org/web/packages/leaflet/index.html
53. Basille M, Bucklin D, Cidre González A. rpostgis: R Interface to a "PostGIS" Database. 2016. Available from: https://CRAN.R-project.org/package=rpostgis
54. Martello E, Yogeswaran G, Reithinger R, Leonardi-Bee J. Mosquito aquatic habitat modification and manipulation interventions to control malaria. Cochrane Database Syst Rev. 2022;11:CD008923.
55. Jacups S, Kurucz N, Whitters R, Whelan P. Habitat modification for mosquito control in the Ilparpa Swamp, Northern Territory. Australia J Vector Ecol. 2011;36:292–9.
56. Dröge S, Poudyal M, Hockley N, Mandimbiniaina R, Rasoamanana A, Andrianantenaina NS, et al. Constraints on rice cultivation in Eastern Madagascar: which factors matter to smallholders, and which influence food security? Hum Ecol. 2022;50:493–513.
57. Laborte AG, Gutierrez MA, Balanza JG, Saito K, Zwart SJ, Boschetti M, et al. RiceAtlas, a spatial database of global rice calendars and production. Sci Data. 2017;4: 170074.
58. Debrah I, Afrane YA, Amoah LE, Ochwedo KO, Mukabana WR, Zhong D, et al. Larval ecology and bionomics of *Anopheles funestus* in highland and lowland sites in western Kenya. PLoS ONE. 2021;16: e0255321.
59. Robert V, Goff GL, Ariey F, Duchemin J-B. A possible alternative method for collecting mosquito larvae in rice fields. Malar J. 2002;1:4.
60. Pock Tsy J-ML, Duchemin J-B, Marrama L, Rabarison P, Le Goff G, Rajaonarivelo V, et al. Distribution of the species of the *Anopheles gambiae* complex and first evidence of Anopheles merus as a malaria vector in Madagascar. Malar J. 2003;2:33.
61. Zohdy S, Derfus K, Headrick EG, Andrianjafy MT, Wright PC, Gillespie TR. Small-scale land-use variability affects *Anophele*s spp. distribution and concomitant *Plasmodium* infection in humans and mosquito vectors in southeastern Madagascar. Malar J. 2016;15:114.
62. Chan K, Konan KA-C, Doudou DT, Kouadio GB, Lines J, Aunger R, et al. Rice farmers' knowledge, attitudes and practices towards mosquitoes in irrigation schemes in Côte d'Ivoire: a qualitative study. Malar J. 2023;22:352.
63. Plank S, Jüssi M, Martinis S, Twele A. Mapping of flooded vegetation by means of polarimetric Sentinel-1 and ALOS-2/PALSAR-2 imagery. Int J Remote Sens. 2017;38:3831–50.
64. Tsyganskaya V, Martinis S, Marzahn P, Ludwig R. Detection of temporary flooded vegetation using Sentinel-1 time series data. Remote Sens. 2018;10:1286.
65. Song M, Xu L, Ge J, Zhang H, Zuo L, Jiang J, et al. EARice10: A 10 m Resolution Annual Rice Distribution Map of East Asia for 2023. ESSD – Land/Land Cover and Land Use; 2024. Available from: https://essd.copernicus.org/preprints/essd-2024-331/
66. Hardy A, Ettritch G, Cross DE, Bunting P, Liywalii F, Sakala J, et al. Automatic detection of open and vegetated water bodies using Sentinel 1 to map African malaria vector mosquito breeding habitats. Remote Sens. 2019;11:593.
67. Rakotoarison HA, Rasamimalala M, Rakotondramanga JM, Ramiranirina B, Franchard T, Kapesa L, et al. Remote Sensing and Multi-Criteria Evaluation for Malaria Risk Mapping to Support Indoor Residual Spraying Prioritization in the Central Highlands of Madagascar. Remote Sensing. 2020;12:1585.
68. Herfort B, Lautenbach S, Porto De Albuquerque J, Anderson J, Zipf A. A spatio-temporal analysis investigating completeness and inequalities of global urban building data in OpenStreetMap. Nat Commun. 2023;14:3985.
69. Google Research. Mapping Africa's Buildings with Satellite Imagery. Google Research. 2024. Available from: http://sites.research.google/gr/open-buildings/
70. Chang Y-L, Tan T-H, Chen T-H, Chuah JH, Chang L, Wu M-C, et al. Spatial-Temporal Neural Network for Rice Field Classification from SAR Images. Remote Sens. 2022;14:1929.
71. Pérez-Carabaza S, Boydell O, O'Connell J. Habitat classification using convolutional neural networks and multitemporal multispectral aerial imagery. JARS. 2021;15: 042406.
72. Hardy A, Oakes G, Hassan J, Yussuf Y. Improved use of drone imagery for malaria vector control through technology-assisted digitizing (TAD). Remote Sens. 2022;14:317.
73. Kahamba NF, Okumu FO, Jumanne M, Kifungo K, Odero JO, Baldini F, et al. Geospatial modelling of dry season habitats of the malaria vector, *Anopheles funestus*, in south-eastern Tanzania. Parasit Vectors. 2024;17:38.

Publisher's Note